dipole array antenna, IEEE Trans Antennas Propagat 52 (2004), 624–628.
9. K.L. Wong, Planar antennas for wireless communications, Wiley, New York, 2003, p. 219.
10. F.R. Hsiao and K.L. Wong, Omnidirectional planar folded dipole antenna, IEEE Trans Antennas Propagat 52 (2004), 1898–1902.
11. A. Nesic and D. Nesic, Omnidirectional uniplanar electromagnetically coupled antenna array, Microwave Opt Technol Lett 40 (2004), 516–518.
12. R. Bancroft and B. Bateman, An omnidirectional planar microstrip antenna with low sidelobes, Microwave Opt Technol Lett 42 (2004), 68–69.

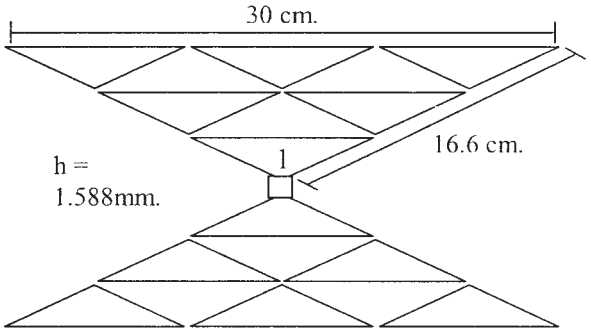

Figure 1 Reconfigurable antenna structure

MODELING FREQUENCY RECONFIGURABLE ANTENNA ARRAY USING NEURAL NETWORKS

Amalendu Patnaik,[1] Dimitrios Anagnostou,[1] Christos G. Christodoulou,[1] and James C. Lyke[2]
[1] Department of Electrical and Computer Engineering
The University of New Mexico
Albuquerque, NM 87131
[2] Air Force Research Laboratory/VSSE
Kirtland AFB
Albuquerque, NM

Received 16 July 2004

ABSTRACT: *In order to avoid the computational complexities involved in analyzing reconfigurable antennas, neural networks are used as an alternate approach. The neural network finds the location of the operational frequency bands for any combination of switches connecting different radiating elements. The network outputs are compared with the experimentally measured results.* © 2005 Wiley Periodicals, Inc.
Microwave Opt Technol Lett 44: 351–354, 2005; Published online in Wiley InterScience (www.interscience.wiley.com). DOI 10.1002/mop.20632

Key words: *antenna array; MEMS; neural networks; reconfigurable antennas*

1. INTRODUCTION

Reconfigurable patch antennas have drawn a lot of attention recently as a paradigm for generating several different antenna-array operating modes with a single reconfigurable antenna structure. These antennas are attractive for many military and commercial applications where it is desirable to have a single antenna structure that can be dynamically reconfigured to transmit and/or receive on multiple frequency bands. In response to antenna-bandwidth needs, significant effort is currently underway to develop reconfigurable antenna systems. Reconfigurable antenna arrays are complex electromagnetic structures comprised of planar radiators that are switched using a network of switches. Due to the multiscale nature of these structures, their numerical modeling poses serious computational challenges. Accurate modeling of the underlying physical phenomena of these structures is extremely important. For accurate modeling of the reconfigurable antenna arrays, one must resort to rigorous full-wave numerical techniques, which demands heavy computing resources. In this paper, an effort has been made to model an MEMS-switched frequency-reconfigurable antenna array (Fig. 1) using artificial neural networks (ANNs). ANNs have emerged in recent years as a powerful technique for modeling general input/output relationships. The distinguished characteristics of ANNs, such as learning from data, for generalizing patterns in data and modeling nonlinear relationships, makes them good candidates for many different branches of engineering.

2. PROBLEM FORMULATION

The MEMS switch-based reconfigurable antenna [1] under investigation is shown in Figure 1. The basic antenna is a 130° balanced bowtie. The reason for choosing this structure for modeling is two-fold. Firstly, with regard to the multiband behaviour of fractal Sierpinski antenna [2], the first six elements on both sides of the feeding point of the antenna correspond to the Sierpinski antenna with two iterations. The remaining six elements are added (three elements on each side) in order to make the antenna a more generalized reconfigurable structure. Secondly, the broader angles move the operating bands to lower frequencies, which can be useful for reducing the antenna height. In addition, the input resistance and reactance variations become smoother when opening the flare angle [3, 4].

The antenna was fabricated on polyethylene substrate ($\varepsilon_r = 2.33$) with no radiating element touching to their adjacent elements. The electromagnetic performance of the RF MEMS switches is considered ideal and their placement is accomplished by small physical connections of the antenna's adjacent conducting parts. Setting all the switches to the OFF state, the antenna has a bandwidth from 1.2 to 2.4 GHz [see Fig. 4(a)], and the radiation pattern is similar to that of the printed bowtie dipole antenna. But here it has to be noted that, in the case of "all switches OFF" the mutual-coupling effect between the elements is found in addition to the characteristics of a simple bowtie. Setting the switches to ON makes the antenna resonate at a number of different frequencies, which include the fractal Sierpinski modes also. The frequencies at which the antenna resonates is completely a function of the switch positions at the ON state. In order to implement this nonlinear function, here we use a multilayer perceptron network trained in the backpropagation mode [5], where the weight updation takes place according to the following equation:

$$w_{ih}^{k+1} = w_{ih}^{k} - \eta \frac{\partial E^k}{\partial w_{ih}}, \tag{1}$$

where η is the learning rate and E^k is the mean square error at the k^{th} instant.

The network (Fig. 2) takes 0s (for an OFF switch) and 1s (for an ON switch) in a specific sequence and presents the S_{11} as its output at the prespecified sampled points. The order in which the switch positions are chosen starts from element 1 and different angles are seen, as shown in Figure 3, keeping in mind that no pairs of elements connecting the switches will be duplicated. A

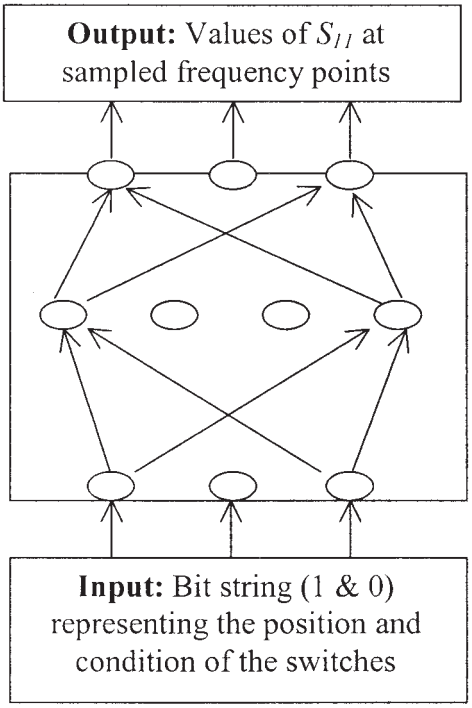

Figure 2 The neural-network topology

total of 18 bits (0 or 1) cover the entire 12 elements of the antenna array and its surrounding switch positions.

3. ANN IMPLEMENTATION

3.1. Data Generation

For different combinations of switches, the S_{11} values of the antenna were measured using a HP8714ES network analyzer in the frequency range of 0.1 to 3 GHz. The measurements were taken for the symmetric combination of switches (symmetric with regard to either of the two vertical planes perpendicular to the plane of the antenna and passing through the feeding point) in order to maintain the radiation pattern of the antenna similarly to that of a dipole for all switch combinations. The S_{11} pattern is then sampled at equidistant points to generate the target data of the neural network for different combination of switches. It was found that at least 40 sampled points adequately represent (note all the -10-dB points) the S_{11} plot.

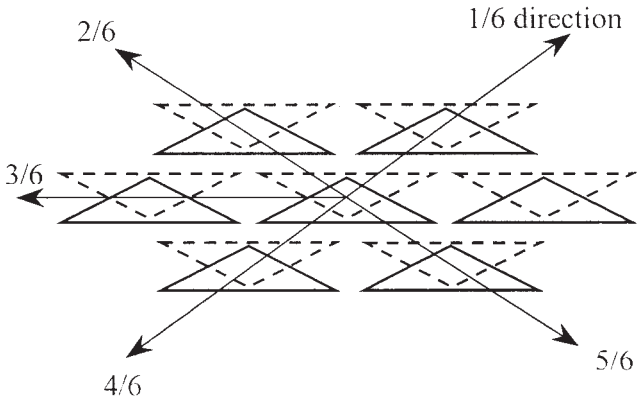

Figure 3 Order in which the elements are chosen to create the input data for the neural network

TABLE 1 Network/Training Parameters

Parameters	Values
Number of input neurons	18
Number of output neurons	40
Number of hidden layers	1
Number of hidden-layer neurons	22
Learning rate (η)	0.05
Performance ratio (γ)	0.7
Training tolerance	1×10^{-2}
Training time (on a 66-MHz P4)	45 min.

3.2. Network Training

The neural network learns from samples of input–output data, that is, a_k and b_k, $k = 1, 2, \ldots, N$, where N is the total number of samples for training. In the present problem, the S_{11} pattern is measured for all 158 different combination of switches ($N = 158$). Because the network size is large compared to the number of available training patterns, in order to avoid a possible overfitting and to improve network generalization, we adopted the regularization method [6]. In this procedure, the performance function of the feedforward network is modified by adding a term with a mean square error that consists of the mean of the sum of the squares of the network weights and biases. The performance function now becomes

$$E = \gamma\left[\frac{1}{N}\sum_{i=1}^{N}(t_i - a_i)^2\right] + (1-\gamma)\left[\frac{1}{n}\sum_{j=1}^{n} w_j^2\right], \qquad (2)$$

where γ is the performance ratio, t_i is the target output, a_i is the network output, and n is the total number of weights and biases.

To implement this, the network inputs and outputs were preprocessed so that they fell approximately in the range $[-1, 1]$.

3.3. Training Parameters

The efficiency of training depends on the training parameters. The values of the training parameters taken for the training of the present network are given in Table 1.

4. RESULTS AND OBSERVATION

The trained neural network was tested for different combination of switches. The results for the structures with different number of active elements are shown in Figures 4(a)–(f). The neural network outputs are compared with the experimental values. As observed from the curves, they are almost in agreement with the experimental results.

As one expects, with the increase in the number of active elements, operating bands in lower frequencies arise [see Figs. 4(a)–(c), (e)] due to the increase in the effective length of the antenna. But this is not always the case, as is evident from Figure 4(d). This may be due to the coupling of the adjacent parasitic elements. It may be pointed out here that the existence of a frequency band not only depends upon the active elements, but also upon the way it has been activated with regard to the other elements, because an element can be activated in many different ways. In other words, the usable frequency ranges of the antenna are a function of the state of the switch (either ON or OFF) and their positions. This is the reason which prompted us to resort to neural networks for the analysis of the structure.

Another point to observe here is that the most of the current density concentrates on the edges of the different triangles that comprise antenna. To verify this, we compared the S_{11} pattern of

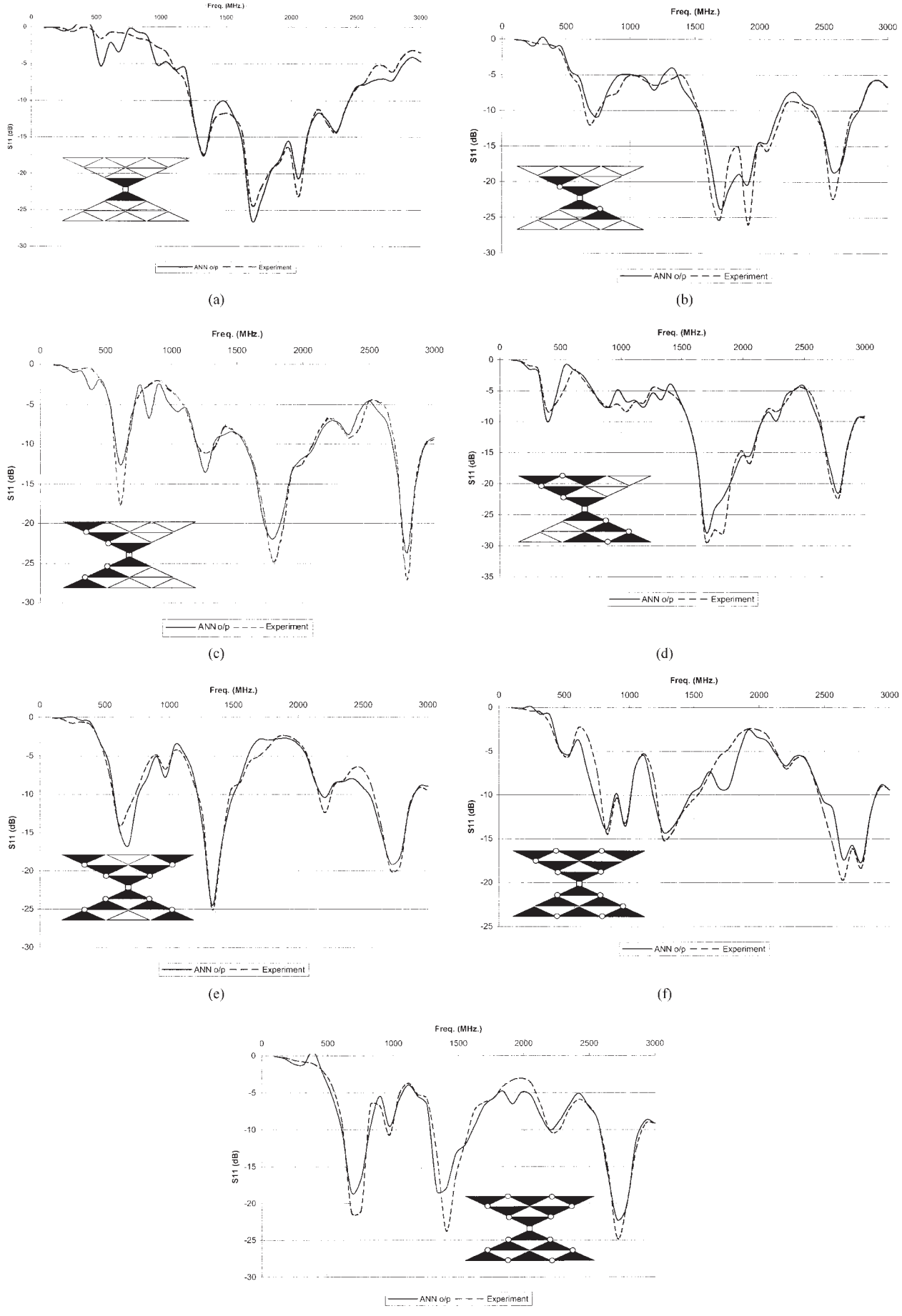

Figure 4 (a)–(g) Plots showing the neural network output as compared to the experimental results (the ON switch positions on the antenna structure are marked with small open circles and the corresponding activated array elements are marked with small filled triangles)

the structure in Figure 4(f) with that in Figure 4(g), in which all the radiating elements are activated, but with a different combination of switches. The prominence of the operating bands can be seen in Figure 4(g).

5. CONCLUSION

A backpropagation neural network is used to locate the operational frequency bands of a MEMS switch-based frequency-reconfigurable antenna. The results show excellent agreement with the experimental values. The developed network can be used to locate the usable frequency bands of the antenna for any combination of switches connecting individual radiating elements of the antenna. This technique drastically reduces the computational complexities involved in the numerical modeling of reconfigurable antennas. The approach can also be extended to the modeling of other reconfigurable structures.

ACKNOWLEDGMENT

A. Patnaik thanks Department of Science & Technology (DST), Govt. of India for awarding him the BOYSCAST Fellowship, during which this work has been done.

REFERENCES

1. D. Anagnostou, M. Khodier, J.C. Lyke, and C.G. Christodoulou, Fractal antenna with RF MEMS switches for multiple frequency applications, Proc 2002 IEEE AP/URSI Symp, San Antonio, TX, 2002, pp. 22–25.
2. C. Puente, J. Romeu, R. Pous, and A. Cardama, On the behaviour of the Sierpinski multiband antenna, IEEE Trans Antennas Propagat 46 (1998), 517–524.
3. C. Puente, M. Navarro, J. Romeu, and R. Pous, Variations on the fractal Sierpinski antenna flare angle, Proc 1998 IEEE AP/URSI Symp, 1998, Atlanta, GA, pp. 2340–2343.
4. C.P. Baliarda, C.B. Borau, M.N. Rodero, and J.R. Robert, An iterative model for fractal antennas: Application to the Sierpinski gasket antenna, IEEE Trans Antennas Propagat 48 (2000), 713–719.
5. S. Haykins, Neural networks: A comprehensive foundation, IEEE Press/IEEE Computer Society Press, New York, 1994.
6. H. Demuth and M. Beale, Neural network toolbox for use with Matlab: User's guide (vers. 4), The Math Works Inc., Natick, MA, 2000.

MFIE MoM-FORMULATION WITH CURL-CONFORMING BASIS FUNCTIONS AND ACCURATE KERNEL INTEGRATION IN THE ANALYSIS OF PERFECTLY CONDUCTING SHARP-EDGED OBJECTS

Eduard Ubeda and Juan M. Rius
Universitat Politècnica de Catalunya (UPC)
Dept. of Signal Theory and Communications (TSC)
Campus Nord UPC, D-3
C/Jordi Girona, 1-3
08034 Barcelona, Spain

Received 10 July 2004

ABSTRACT: *We present a novel technique to integrate analytically the highest-order terms of the Kernel of a low-order curl-conforming magnetic-field integral equation (MFIE) operator. In the computation of the bistatic RCS of moderately small perfectly conducting sharp-edged examples, we show that this curl-conforming choice yields very similar performance to that of the MoM-EFIE formulation and outperforms a MoM-MFIE formulation based on the RWG basis functions, both with very accurate Kernel integration.* © 2005 Wiley Periodicals, Inc. Microwave Opt Technol Lett 44: 354–358, 2005; Published online in Wiley InterScience (www.interscience.wiley.com). DOI 10.1002/mop.20633

Key words: *method of moments; integral equation techniques; basis functions; electromagnetic scattering; radar cross section*

1. INTRODUCTION

The most useful basis functions in computational electromagnetics may be classified in two general groups. The divergence-conforming basis functions ensure the continuity of the normal component of the current across the borders of the elements of the discretization. The curl-conforming set enforces the tangential component of the current to be continuous [1, 2].

Very well-known method of moments (MoM) formulations for EFIE [3] and MFIE [4] for PeC objects make use of RWG basis functions, which are low-order examples of a divergence-conforming set. Similarly, a low-order curl-conforming set has also been used in the analysis of PeC objects [5, 6]. In the MoM formulations for the analysis of penetrable objects, where the operators come from linear combinations of the EFIE and MFIE operators in the PeC case, RWG basis functions have been used to expand both the electric and magnetic currents [7]. Moreover, MoM formulations for the analysis of complex objects with dielectric and perfectly conducting regions recommend the use of coupled sets of basis functions, thus expanding the electric and magnetic currents with the RWG basis functions and the corresponding low-order curl-conforming set [8], respectively.

In the numerical analysis of moderately small sharp-edged objects—with dimensions of about 0.1λ—the EFIE operator with RWG basis functions has been successfully used [3]. However, the use of the RWG basis functions with the MFIE operator produces a remarkable discrepancy with respect to the EFIE operator. This error can be diminished to some extent through a heuristical correction of the solid angle [9]. This disagreement can be best perceived for moderately small sharp-edged objects because the relative effect of the edges on the scattered fields is more important. In this paper, numerical examples show that the curl-conforming choice for the basis functions in the MFIE formulation with very accurate integration of the Kernel works better than the conventional divergence-conforming choice.

2. DIVERGENCE-CONFORMING EFIE AND MFIE

The formulations for the electric-field integral equation (EFIE) and the magnetic-field integral equation (MFIE) are derived from the electric- and magnetic-field boundary conditions over the surface of the scatterer, respectively:

$$\vec{J} = \hat{n} \times \vec{H} = \hat{n} \times \vec{H}^i + \hat{n} \times \vec{H}^s, \tag{1.1}$$

$$0 = [\vec{E}^i + \vec{E}^s]_{\tan}, \tag{1.2}$$

where $\hat{n}$ denotes the normal vector to the surface of the scatterer and $\vec{E}^i$, $\vec{H}^i$ and $\vec{E}^s$, $\vec{H}^s$ stand for the incident and the scattered fields, respectively. By $[\ ]_{\tan}$ we mean the field component tangential to the surface.

The integro-differential expressions used to compute the scattered magnetic and electric fields above in terms of the electric current-surface density $\vec{J}$ are given by